International Journal of Biological Macromolecules 244 (2023) 125312

Contents lists available at ScienceDirect

International Journal of Biological Macromolecules

journal homepage: www.elsevier.com/locate/ijbiomac

Interactions of ultrashort laser pulses with hemoglobin: Photophysical aspects and potential applications

Mihajlo D. Radmilović [a], Ivana T. Drvenica [b], Mihailo D. Rabasović [a], Vesna Lj. Ilić [b], Danica Pavlović [a], Sho Oasa [c], Vladana Vukojević [c], Mina Perić [d,e], Stanko N. Nikolić [a,f], Aleksandar J. Krmpot [a,f,*]

[a] Institute of Physics Belgrade, University of Belgrade, Belgrade, Serbia
[b] Institute for Medical Research, National Institute of Republic of Serbia, University of Belgrade, Belgrade, Serbia
[c] Department of Clinical Neuroscience, Karolinska Institutet, Stockholm, Sweden
[d] Faculty of Biology, University of Belgrade, Belgrade, Serbia
[e] Institute of Molecular Genetics and Genetic Engineering, University of Belgrade, Belgrade, Serbia
[f] Division of Arts and Sciences, Texas A&M University at Qatar, Doha, Qatar

ARTICLE INFO

Keywords:
Erythrocytes
Two-photon excitation fluorescence
Hemoglobin photoproduct
Femtosecond laser
Protoporphyrin IX

ABSTRACT

Hemoglobin (Hb), a life-sustaining and highly abundant erythrocyte protein, is not readily fluorescent. A few studies have already reported Two-Photon Excited Fluorescence (TPEF) of Hb, however, the mechanisms through which Hb becomes fluorescent upon interaction with ultrashort laser pulses are not completely understood. Here, we characterized photophysically this interaction on Hb thin film and erythrocytes using fluorescence spectroscopy upon single-photon/two-photon absorption, and UV-VIS single-photon absorption spectroscopy. A gradual increase of the fluorescence intensity, ending up with saturation, is observed upon prolonged exposure of Hb thin layer and erythrocytes to ultrashort laser pulses at 730 nm. When compared to protoporphyrin IX (PpIX) and oxidized Hb by H_2O_2, TPEF spectra from a thin Hb film and erythrocytes showed good mutual agreement, broad peaking at 550 nm, supporting hemoglobin undergoes degradation and that same fluorescent specie(s) originating from the heme moiety are generated. The uniform square shaped patterns of the fluorescent photoproduct exhibited the same level of the fluorescence intensity even after 12 weeks from the formation, indicating high photoproduct stability. We finally demonstrated the full potential of the formed Hb photoproduct with TPEF scanning microscopy towards spatiotemporally controlled micropatterning in HTF and single human erythrocyte labelling and tracking in the whole blood.

1. Introduction

Human adult hemoglobin (Hb) is an iron-containing metalloprotein in erythrocytes, the primary function of which is to transport oxygen from the lungs to all other organs and tissues. It is made up of two α- and two β-polypeptide chains, each associated with one hem prosthetic group [1]. While the absorption spectrum of oxyhemoglobin (oxyHb) shows several bands, as the intense Soret or B band in the region of 370 nm - 450 nm and the so-called Q-band in the region of 500 nm – 650 nm in the porphyrin ring [2], the conventional single-photon excitation fluorescence (SPEF) of Hb is not or hardly detectable due to the fast non-radiative decay that dominates over spontaneous fluorescence emission [3–5]. In contrast, the intense two-photon absorptivity of Hb in the near-infrared range [6] followed by strong fluorescence emission, have made Two-Photon Excited Fluorescence (TPEF) imaging possible [4] and applicable in a number of studies: for erythrocytes imaging [7,8], analysis of residual Hb distribution in empty erythrocytes membranes (i.e., erythrocyte ghosts) [9], in vivo imaging of microvasculature [10–12], and even time-resolved diagnostic imaging [13]. Of note, Hb excitation through a two-photon absorption process, which is governed by significantly different selection rules than single photon absorption, is described in detail in [3,5], while the corresponding single and two photon absorption spectra are given in [6].

Due to high absorptivity of Hb in the VIS and near infrared (NIR) region, erythrocytes are also readily imaged using absorption-based techniques, such as photo-acoustic microscopy [14]. Photo-acoustic

* Corresponding author: Institute of Physics Belgrade, University of Belgrade, Belgrade, Serbia, Pregrevica 118, Belgrade 11080, Serbia.
E-mail address: krmpot@ipb.ac.rs (A.J. Krmpot).

https://doi.org/10.1016/j.ijbiomac.2023.125312
Received 21 March 2023; Received in revised form 16 May 2023; Accepted 8 June 2023
Available online 10 June 2023

microscopy is an imaging technique that leverages the non-radiative decay of Hb, which happens to be the most frequently used contrast agent for this modality [15–17]. Another type of label free imaging techniques, used for erythrocytes imaging is the nonlinear Third Harmonic Generation (THG) microscopy. This method has demonstrated efficacy in imaging erythrocytes contained within transfusion bags. [18].

The significance of photochemical manipulation of proteins is especially boosted by the discoveries of their optogenetics, photobiomodulation and bioimaging applications in recent years [19,20]. Understanding the photophysical and photochemical processes during the interaction of Hb with ultrashort laser pulses is of great importance for the development of functional imaging aimed for the assessment of erythrocytes functional status [21], where hemoglobin is the main intracellular protein of these cells. Besides, a better understanding of the interaction of Hb with ultrashort laser pulses could contribute to the development of new methods for the characterization and tracking of extracellular Hb presence. This implies extracellular Hb from endogenous sources due to hemolysis (in all diseases where in common feature is hemoglobinemia, such retinopathy, neuropathy, nephropathy and brain hemorrhages) [22], or exogenous sources, such in the cases of use of hemoglobin-based oxygen carriers [23] and hemoglobin-based drug delivery system, which have great potential in cancer therapy [22,24,25]. So far it was only shown that upon ultrashort laser pulses interaction with Hb, there is relation between TPEF spectra of heme and hemoglobin, as stated in [3].

However, despite already established, as well as emerging applications of Hb-based TPEF microscopy, the origin of generated fluorescence still needs to be completely understood. While it was initially proposed that the origin of the observed Soret fluorescence (420–460 nm) with a fluorescence emission peak at 438 nm originates from Hb [3], it was shown that TPEF does not directly originate from Hb, but rather from a photoproduct created upon the interaction of ultrashort laser pulses used in this nonlinear imaging technique with Hb [26]. This lack of basic understanding motivated us to deeper study ultrashort laser pulses interaction with Hb, with a particular focus on characterizing the durability of the Hb photoproduct and experimental conditions under which it is being formed. Since we efficiently demonstrated utility of TPEF microscopy to image the erythrocytes, the ultrashort laser pulses interaction with Hb was further photophysically characterized on thin Hb films using fluorescence spectroscopy upon two-photon absorption, UV-VIS single-photon absorption spectroscopy, and spectral fluorescent imaging. To examine whether degradation of the heme moiety occurs when ultrashort laser pulses used in TPEF microscopy imaging interact with Hb, spectroscopic properties of heme precursor protoporphyrin IX (PpIX), a heterocyclic organic compound that consists of four pyrrole rings, were analyzed. In addition, photophysical properties of the Hb photoproduct were compared to photophysical properties of compound (s) formed under Hb oxidation with hydrogen peroxide (H_2O_2) [27,28] to determine whether there are differences in the optical response of products formed under chemically induced Hb degradation. Finally, we examined the potential of the Hb photoproduct to be used for micropatterning and single erythrocyte tracking.

2. Materials and methods

2.1. Sample collection and processing

Venous blood from healthy human volunteer was collected at the Institute for Transfusiology and Hemobiology, Military Medical Academy, Belgrade, Serbia. The protocol was approved by the Institutional Ethical Review Board (No 9/2021). In conformance with the World Medical Association Declaration of Helsinki, informed consent was obtained from potential participants. The blood was drawn using vacutainer tubes (10 mL plastic vacutainer (BD Vacutainer® EDTA Tubes) with BD Hemogard™ lavender closure containing 18 mg K2EDTA). To prepare slides for direct TPEF microscopy imaging of erythrocytes, 10 μL of whole blood was diluted in isotonic saline solution (0.9 % NaCl, Natrii chloridi infundibile 9 g/L, Hemofarm, Serbia) in the volume: volume ratio 1:30. 3 μL of diluted whole blood sample was smeared onto a microscope slide, covered by a No. 1.5 coverslip and sealed.

2.2. Hb isolation

To isolate hemoglobin, human erythrocytes were precipitated by whole blood centrifugation. To this aim, 10 mL of whole blood was centrifuged at 1811 $\times g$ for 20 min at 4 °C (Megafuge 1.0R, Heraus centrifuge, Langenselbold, Germany). The supernatant, consisting of leucocytes in plasma, was carefully removed by aspiration and discarded. The precipitated erythrocytes were resuspended in isotonic saline solution (0.9 % NaCl, Natrii chloridi infundibile 9 g/L, Hemofarm, Serbia) in a volume:volume ratio of 1:4 and the suspension was homogenized by fine twisting the test tube. The remaining plasma proteins were removed by centrifugation of the erythrocyte suspension at 1257 $\times g$ for 10 min at 4 °C. These steps were repeated three times. Finally, the precipitated erythrocytes (packed) were resuspended in the isotonic phosphate buffered saline solution (PBS; 0.8 % saline buffered with 10 mM sodium phosphate, pH 7.2–7.4) in the volume: volume ratio of 1:4.

The hemolysis of erythrocytes suspension was performed using hypotonic 5 mM sodium phosphate buffer, pH 7.2, at 4 °C. Specifically, in 1 mL of erythrocytes suspension in PBS, 9 mL of 5 mM sodium phosphate buffer was added, and the tube was slightly mixed and then left at 4 °C for 1 h. The suspension was centrifuged at 3220 $\times g$ for 40 min at 4 °C. After centrifugation, the supernatant fluid containing released Hb molecules was collected, and the aliquots were filtered through 0.2 μm syringe filter. If not used immediately, the samples of Hb were aliquoted and stored at −20 °C for future use. Just before the experiment, a Hb aliquot would be thawed, and its concentration checked. Only one freeze-thaw cycle was allowed so the aliquots were discarded after experiment performed. All tests were done with Hb stored for less than two years from Hb isolation, since our previous results showed that it remains intact-undecomposed and non-aggregated under these storage conditions [29].

2.3. Hb thin film preparation for TPEF microscopy imaging

Thin Hb films were prepared by smearing 5 μL of Hb on the microscope slide, air-drying for 3 min and covered by No. 1.5 coverslip and sealed. The film thickness was <50 μm, as measured by confocal laser scanning microscopy, i.e., scanning along the z-axis. The smallest step of motorized the microscope stage stepper motor was 0.3 μm.

2.4. Protoporphyrin IX (PpIX) thin film preparation for TPEF microscopy imaging

Protoporphyrin IX (PpIX) in the form of a disodium salt was purchased from Sigma Aldrich (USA) and used without further purification. 20 μM stock solution of PpIX was prepared by dissolving 0.1 g of PpIX in 1 M HCl to the total volume of 50 mL. The stock solution was stored at 25 °C protected from light, to minimize photo-induced degradation of PpIX. To prepare slides for TPEF spectroscopy and spectral imaging, the PpIX stock solution was diluted in 1 × PBS (Sigma Aldrich, 140 mM NaCl, 10 mM phosphate buffer, and 3 mM KCl, pH 7.4) to the final concentration of 5 μM. 5 μL of this solution was placed on a microscope slide and treated in the same way as for Hb thin film preparation described above.

2.5. TPEF imaging of Hb treated with H_2O_2

The 22.5 M H_2O_2 was diluted using PBS (Sigma Aldrich, 140 mM NaCl, 10 mM phosphate buffer, and 3 mM KCl, pH 7.4) to a concentration of 250 μM. Further, 1 mL of Hb at a concentration of 22.3 g/L,

was incubated with 0.5 mL of 250 μM H_2O_2 for 30 min at room temperature (≈ 21 °C). After incubation, 5 μL of this mixture was placed on a microscope slide, smeared, dried, covered by a #1.5 coverslip and sealed.

2.6. TPEF scanning microscopy, micropatterning, and micro-spectroscopy

The experimental setup and home built TPEF microscope have been previously reported [30,31]. In this work, we upgraded it for micropatterning and micro-spectroscopic experiments. Schematic drawing of the experimental setup is shown in Fig. 1. The Ti:Sapphire laser (Coherent, Mira 900-F), pumped by a frequency-doubled Nd:YVO4 laser (Coherent, Verdi V10), was used to generate ultrashort laser pulses with the repetition rate of 76 MHz and pulse duration of 160 fs. Galvo-scanning mirrors (Cambridge Technology) are used for raster scanning and micropatterning. Two microscope objectives were used in this study: EC Plan-NEOFLUAR 40× /1.3 N.A. oil (Carl Zeiss) for erythrocyte imaging and Plan-Apochromat 20× /0.8 N.A. air (Carl Zeiss) for Hb micropattering. The laser beam was expanded to fulfill the back aperture of the objective lens. A short-pass dichroic mirror was used to reflect the laser beam towards the objective lens and transmit the signal to the 15.1-megapixel digital single-lens reflex (DSLR) camera (Canon, EOS 50D) and the Photomultiplier Tube (PMT) (RCA, PF1006). The DSLR camera was used for taking bright-field images. We removed the infrared filter from the camera to see the back reflection of the laser beam from the cover glass for the purpose of system alignment and to facilitate axial positioning of the thin Hb layer. Band pass filters (VIS and/or 450 nm short pass) were placed in front of the PMT to collect Hb photoproduct fluorescence. A 700 nm long pass filter was used to remove parasitic laser lines shorter than 700 nm. A short pass 700 nm filter was placed in front of the PMT detector to additionally remove back scattered laser light. The Hb photoproduct formation and erythrocytes imaging were performed at 730 nm ultrashort laser pulses. This wavelength is chosen as optimal according to the optical setup and properties of Hb molecule, whilst details are given in our previous study [9].

In addition, we were able to record in situ TPEF emission spectra of the Hb photoproduct and erythrocytes using fiber-coupled, thermo-electrically (TE) cooled charge-coupled device (CCD) spectrometer with reduced thermal noise (Glacier X, BWTEK). To collect the TPEF emission from arbitrary chosen excitation point, the fiber was attached to the adapter plate (Thorlabs, S1SMA) mounted on the precise translation stage (Thorlabs, ST1XY-D/M). Henceforth, we refer to the in situ acquisition of TPEF emission spectra from an arbitrarily chosen point in

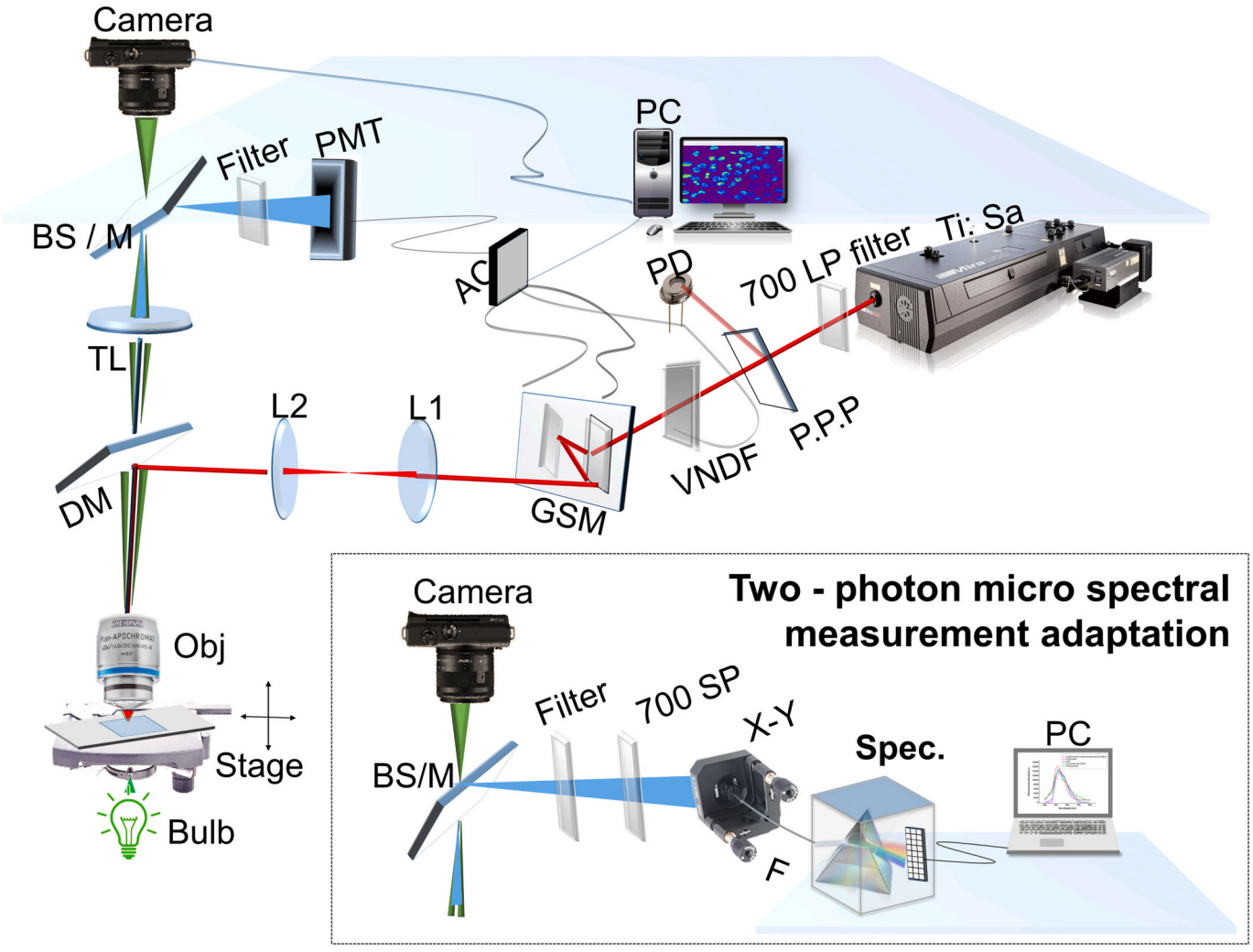

Fig. 1. Schematic 3D drawing of the home-built TPEF microscope with specific adaptations for in situ emission spectra measurement (inset). The TPEF microscope comprising the: Ti:Sa, Ti:Sapphire laser; 700 LP filter, 700 nm long pass filter; P.P.P., plan parallel plate; PD, photo-diode; VNDF, variable neutral density filters; GSM, galvo scanning mirrors; L1 and L2 lenses; AC, acquisition card; DM, dichroic mirror (short pass); Bulb, bulb for bright-field imaging; TL, tube lens; BS/M, beam splitter or mirror; PMT, photomultiplier tube. Inset: The module for micro spectral measurements comprises: 700 SP filter, 700 nm short pass filter; X-Y F, functional X-Y stage controller, Spec, compact high-performance CCD spectrometer with TE cooling.

the sample as micro-spectroscopy. Square-shaped TPEF emission patterns were inscribed by raster-scanning of the sample, whereas arbitrary patterns were inscribed by scanning the beam along a corresponding line. The latter is enabled by a specially written program that recognizes arbitrary figures in both vector, and bitmap formats, and controls the dwell time, power and writing speed of the fs laser beam.

2.7. Single-photon excitation fluorescence (SPEF) and confocal laser scanning microscopy (CLSM)

Hb photoproduct lastingness was assessed by single-photon excitation fluorescence (SPEF) using a confocal laser scanning microscope (LSM 510, Carl Zeiss), equipped with an Ar multi-line (458 nm, 488 nm, and 514 nm) laser and a Plan Apochromat 40 × 1.3 N.A. oil-immersion objective (Carl Zeiss). Optical slice thickness was set to <4.3 μm, by choosing the pinhole diameter of 5.65 Airy units, to collect as much as possible fluorescence light from the photoproduct and to increase Signal to noise ratio (SNR). The best signal-to-noise-ratio in the SPEF images of the Hb photoproduct in the square-shaped patterns was at 488 nm excitation wavelength. Emission was collected using the main dichroic beam splitter, HFT 488 nm and long pass filter LP 505 nm.

2.8. Absorption spectra measurements

Absorption spectra of Hb and TPEF irradiated Hb in the intact thin film were measured using the Beckman Coulter DU700 spectrophotometer. A special aluminum holder was designed to hold the microscope slide with Hb specimen, to mimic a cuvette for the spectrophotometer. The dimensions of the holder were 45 mm × 10 mm × 10 mm. The mask with the round hole was placed over the cover glass with Hb layer and photoproduct square pattern. The hole matches the Hb photoproduct enabling the portion of incident light from the spectrophotometer to pass only through the region where the Hb photoproduct is. Prior to the absorption measurements, necessary calibration was performed for the overall transmission.

2.9. Spectral imaging

Spectral confocal Laser Scanning Microscopy (CLSM) imaging was performed using an LSM880 (Carl Zeiss) instrument, equipped with several lasers: three diode lasers (543 nm and 633 nm), and an Ar-ion laser (lines: 458 nm, 488 nm and 514 nm); objective lens (Plan-Apochromat 20×/0.8 N.A.); and gallium arsenide phosphide (GaAsP) spectral array detector. The pinhole size was adjusted to 33 μm (1 Airy unit at 488 nm). The fluorescence (single-photon excitation fluorescence (SPEF)) was spectrally split by a diffraction grating and detected in the 418 nm - 723 nm range with a 3 nm wavelength resolution using the GaAsP spectral array detector. For all wavelengths, the laser power was 9.4 μW at the objective lens. SPEF emission spectra are displayed only for wavelengths that are longer than the wavelength of the excitation laser.

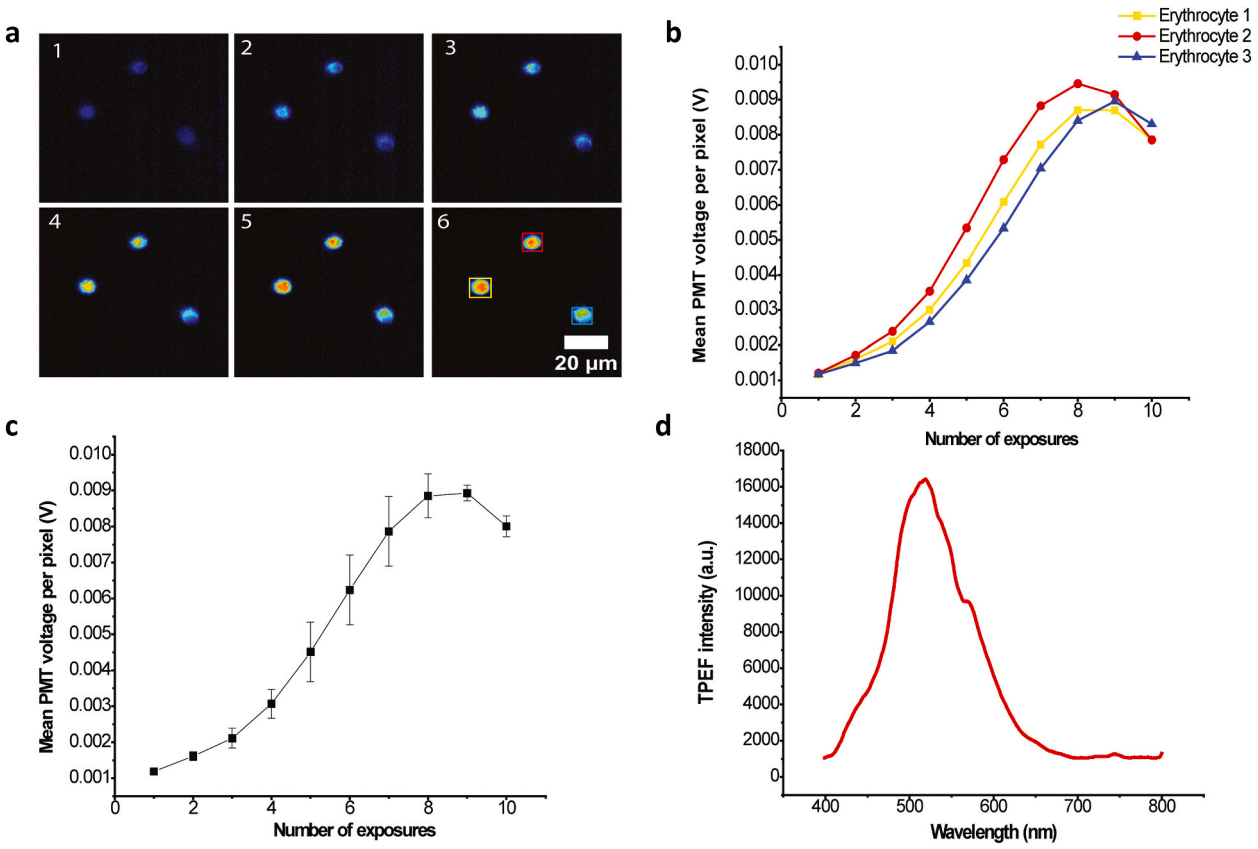

Fig. 2. TPEF microscopy enables both selective erythrocyte photolabeling and imagining in the whole blood. (a) Label-free TPEF microscopy images (6 out of 10) of erythrocytes. The image pixel size is 1024 × 1024 pixels; it is averaged out from 30 scans with the pixel dwell time is 8.53 e^{-4} s. In total, each image took 26.1 s to be recorded, which represents a single unit of exposure. The image intensity is represented by pseudocolor code of PMT voltage values for each pixel (dark blue – lowest TPEF signal, red – highest TPEF signal); (b) Mean pixel values of PMT voltage proportional to the TPEF intensity for each ROI (yellow, red and blue square box) shown in (a)), presented with the curve of the corresponding colour. Mean pixel values were calculated from region of interest (ROI), (yellow, red and blue squares) and for each image, the square size is 100 × 100 pixels; (c) Black curve is average of three erythrocytes shown in (b), standard error was presented for the ordinate (voltage); (d) TPEF spectrum recorded in an arbitrarily selected point in a single erythrocyte, using micro-spectral measurement adaptation. (For interpretation of the references to colour in this figure legend, the reader is referred to the web version of this article.)

3. Results and discussion

3.1. Photo-labeling of erythrocytes using TPEF microscopy and micro-spectroscopy analysis of erythrocytes fluorescence emission

To confirm already demonstrated feasibility of TPEF microscopy for erythrocytes imaging [8,9], we initially performed an analysis on diluted human whole blood. The blood was diluted in order to get sparse erythrocytes that are not stacked to each other and clearly distinguishable at the image. TPEF microscopy allowed us to selectively photo-label individual erythrocytes in a whole blood specimen. Here, photo-labeling refers to the process of rendering fluorescent individual erythrocytes using ultrashort 730 nm laser pulses. The gradual increase of TPEF from the irradiated erythrocytes as the laser beam scans over them is shown in Fig. 2a. This result was in accordance with the already demonstrated increase of the fluorescence intensity in the erythrocytes upon illumination with ultrashort laser pulses and formation of a so called Hb photoproduct [26]. Herein, the increase of TPEF signal has been proven through the PMT voltage dependence on the number of exposures (Fig. 2b), since PMT voltage is directly proportional to the fluorescence intensity. The abscissa shows the number of exposures whereat one exposure refers to a series of 30 consecutive image frames acquired by raster laser scanning, the acquisition of which lasted ~26.1 s. The ordinate shows the mean PMT voltage *per* exposure per pixel of the rectangular regions given in the last image (no.6) at Fig. 2a. The average PMT voltage i.e., fluorescence intensity curve is presented in Fig. 2c. In addition, the TPEF emission spectrum was acquired (Fig. 2d) using a CCD array fiber optic spectrometer mounted on the nonlinear microscope (Fig. 1 inset).

3.2. Hb photoproduct formation using 730 nm ultrashort laser pulses

To ascertain that the observed increase in TPEF intensity comes solely from the Hb photoproduct that was formed upon erythrocytes illumination with ultrashort 730 nm laser pulses, but not from other molecules, we performed experiments using isolated Hb. To this aim, square-shaped patterns were inscribed in the thin Hb film in a spatio-temporally controlled manner: 1024 × 1024 pixels at average laser power of 20 mW (Fig. 3a). Both SPEF (Fig. 3b) and TPEF images (Fig. 3c) were acquired. The acquisition procedure was repeated 10 times

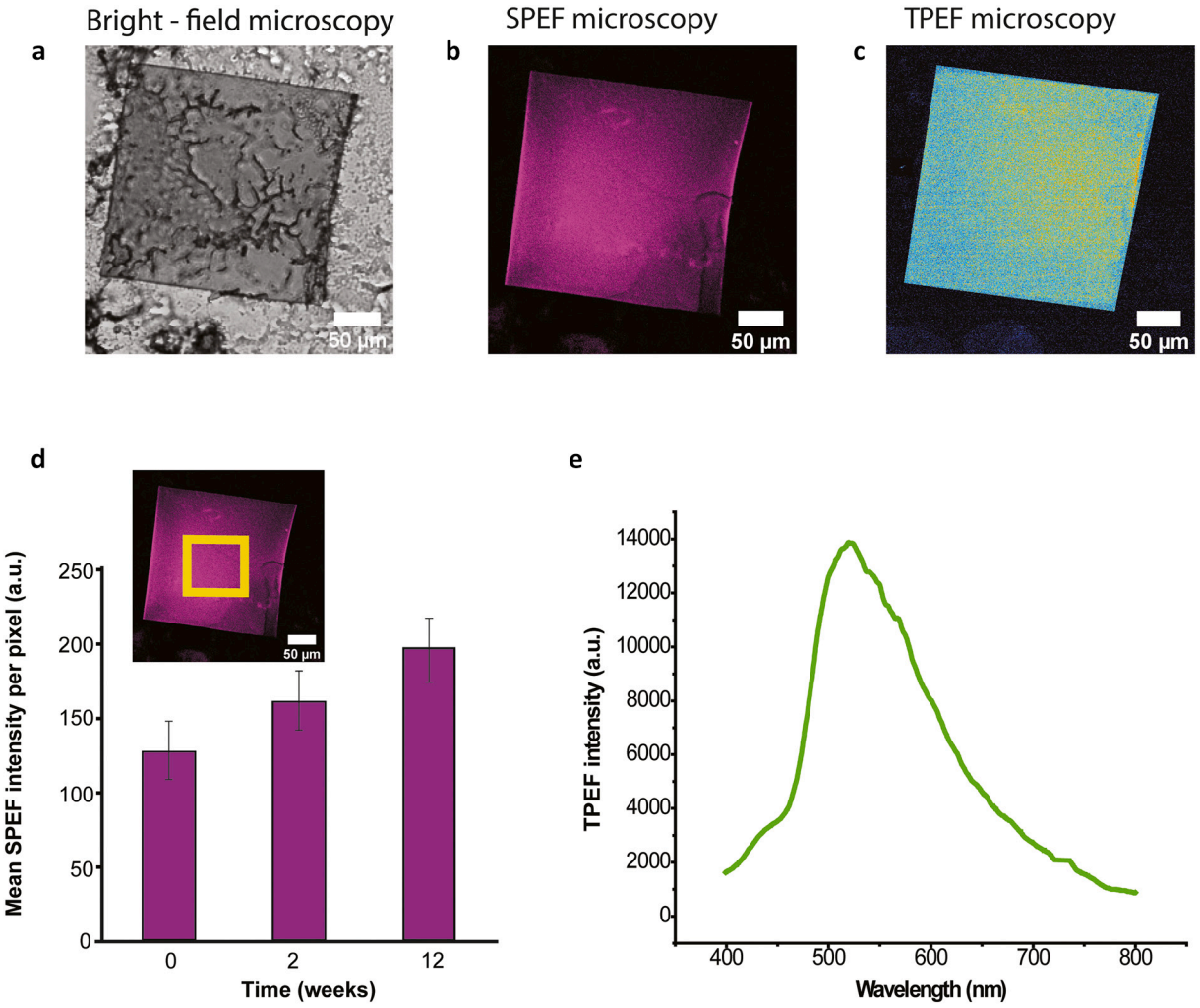

Fig. 3. SPEF spectra of the Hb photoproduct formed upon Hb thin film exposure to ultrashort 730 nm laser pulses. (a) Bright-field microscopy image of the specimen shown reveals that the Hb photoproduct (dark grey square) is less optically translucent than Hb (light grey surrounding); (b) Single-photon excitation fluorescence (SPEF) emission image of the specimen shown in (a) reveals that Hb photoproduct SPEF can be excited at 488 nm (plum square) whereas Hb cannot (black surrounding); (c) Representative TPEF microscopy image showing intense emission in the yellow-green square-shaped area where the Hb photoproduct was formed, in comparison to the non-fluorescent Hb in the surrounding (black); (d) The Hb photoproduct is lasting and its SPEF emission properties are preserved over extended time, as evident from the mean SPEF intensity per pixel (measured in the yellow rectangular area in the inset); (e) TPEF spectrum of the Hb photoproduct recorded in an arbitrarily selected point in the thin layer. (For interpretation of the references to colour in this figure legend, the reader is referred to the web version of this article.)

(number of exposures) after 8 scanning times the maximum TPEF intensity was reached, after that the TPEF intensity started to decrease due to photobleaching (see Fig. 2b). To demonstrate that strong TPEF emission is observed only from the region that was exposed to ultrashort 730 nm laser pulses, the field of view, i.e., the scanned region was expanded, the average laser power was lowered down to 2.5 mW and a TPEF image was acquired (Fig. 3c). In addition, bright field imaging clearly showed that transmission properties of the extensively illuminated square-shaped area have become less transparent (Fig. 3a). Finally, using single-photon excitation at 488 nm, we detected SPEF emission from the Hb photoproduct formed only in the region exposed to ultrashort 730 nm laser pulses, but not in the surrounding region (Fig. 3b, plum). Here, it is worth reminding that Hb is not naturally fluorescent [26], which is obvious from the dark region around the fluorescent square (Fig. 3a and c). The photoproduct formation depends on exposure time and laser average power, among other parameters that are fixed in our experiment (wavelength, repetition rate, pulse duration etc.). The fluorescence intensity signal starts to increase even after the first exposure. For Hb isolated as stated in previous Section 2.2, TPEF intensity of the Hb photoproduct becomes detectable at a laser excitation power of approximately 10 mW after the first exposure, which corresponds to the deposited energy of 261 mJ on the square area 62,500 μm^2.

Similarly, to erythrocytes, the increase in fluorescence intensity was gradual with the number of scanning times (i.e., number of exposures) across the square area which is proportional to the total absorbed dose/energy (plot is equivalent to the plot shown in (Fig. 2b). This suggests that ultrashort laser pulses interact directly with Hb to form photoproduct in the erythrocyte. Longitudinal SPEF recordings showed that the Hb photoproduct is stable over a considerably long time (Fig. 3d). The TPEF spectrum of the Hb photoproduct in the thin film showed maximum at (550 ± 2) nm (Fig. 3e), the same to the TPEF emission spectrum recorded from a single erythrocyte (Fig. 2c). This observation suggests that ultrashort laser pulses interact solely with Hb in the erythrocytes from the whole blood, forming the same photoproduct. Or, at least, one could say that the interaction of the ultrashort laser pulses with other molecular species in erythrocytes is negligible, at the given conditions. The dynamic of Hb photoproduct formation is also the same in erythrocytes and Hb thin film: gradual increase of the fluorescence intensity with number of exposures that end up with saturation plateau. We might anticipate that interaction of ultrashort laser pulses with Hb is mainly followed up with an intensive Hb degradation, due to the increasing fluorescence intensity over time and the eventual saturation of the fluorescence when the majority of Hb in focal volume is degraded.

3.3. UV-VIS absorption spectroscopy of TPEF irradiated and non-irradiated thin Hb layer

To characterize the single-photon absorption spectra of Hb and the TPEF irradiated Hb in the intact thin film, measurements were performed outside and inside the illuminated square-shaped region (Fig. 3a-c), respectively. The term irradiated Hb was used because of the measurement procedure of the absorption spectra. Since photoproduct was formed in a thin layer of Hb film so that both Hb and the photoproduct are on the same optical path. In addition, some Hb remains unconverted into the photoproduct even in the treated volume. That's why the recorded absorption spectrum is not solely from the photoproduct, but from both, photoproduct and Hb together.

As expected, the UV-VIS absorption spectrum of Hb thin film showed spectral bands that are characteristic of oxyHb: an absorption band in the UV region with a maximum at $\lambda_{max}^{UV} \approx$ 275 nm due to $\pi \rightarrow \pi^*$ transitions; and several absorption bands, such as the λ_{max}^{His} 350 nm attributed to the absorption of the non-covalent bond between iron and histidine in the Hb protein part; the Soret or B band λ_{max}^{Soret}at (410 ± 2) nm and the Q band with two transitions, the $\lambda_{max}^{Q\beta}\beta$ band at 539 nm and $\lambda_{max}^{Q\alpha}\alpha$ band at 577 nm [32] (Fig. 4, blue line). Similarly, the UV-VIS absorption spectrum of the TPEF irradiated Hb thin film showed the same bands, but clear differences in band intensity and/or peak position were noted (Fig. 4, red line). The observed differences and important relations between them are summarized in Table 1.

A 7 nm bathochromic shift of the Soret band was noted in the irradiated Hb with a significant decrease in Soret band intensity (Fig. 4, Table 1). The bands in the VIS part of the Hb absorption spectrum originate from the heme group, and changes in their positions and intensities are indicators of displacements along the normal coordinates of the porphyrin ring [33]. The ratio of $\Delta\alpha/\Delta\beta$ was <1 for both Hb and Hb after irradiation with fs laser pulses (Fig. 4, Table 1). Still, this ratio in irradiated Hb was significantly lower than untreated Hb indicating the degradation of Hb upon the interaction with fs laser pulses. The mentioned 7 nm bathochromic shift of the Soret peak in the irradiated Hb, indicates the transformation of oxygenated to oxidized Hb species [33–35]. Reduced ratio A_{max}^{Soret}/A_{560} ratios of irradiated Hb in comparison to intact Hb indicate free heme presence and breakdown of Hb molecule [33].

3.4. Single-photon excitation fluorescence (SPEF) emission spectra of thin film Hb photoproduct by confocal microscopy spectral imaging

The Hb photoproduct square shape patterns are imaged using single-photon excitation confocal microscopy (Fig. 5a), and square shape patterns (Fig. 5b) were formed previously by the exposure to the ultrashort laser pulses as explained in Section 2.9. SPEF emission spectra were recorded for different excitation wavelengths (Fig. 5c) from the Hb region of interest 1 (ROI1, dashed circle) and from the photoproduct region of interest (ROI 2, solid circle). Excitation efficiency dependence was constructed by extracting emission maxima at different excitation wavelengths (Fig. 5d). The SPEF emission spectrum acquired using the shortest excitation wavelength, λ_{exc} = 458 nm, showed a fluorescence emission maximum at λ_{em} = 550 nm and a broad emission band (red curve), being good agreement with TPEF emission spectrum (Fig. 3e). The emission spectra acquired using excitation wavelengths longer than 458 nm, λ_{exc} > 458 nm, showed emission maxima that are slightly red shifted to one another, possibly suggesting that the Hb photoproduct may comprise several spectrally distinct molecules. The existence of more than one molecular species is confirmed by the absorption spectroscopy (Section 3.3) and it is in accordance with the results given in

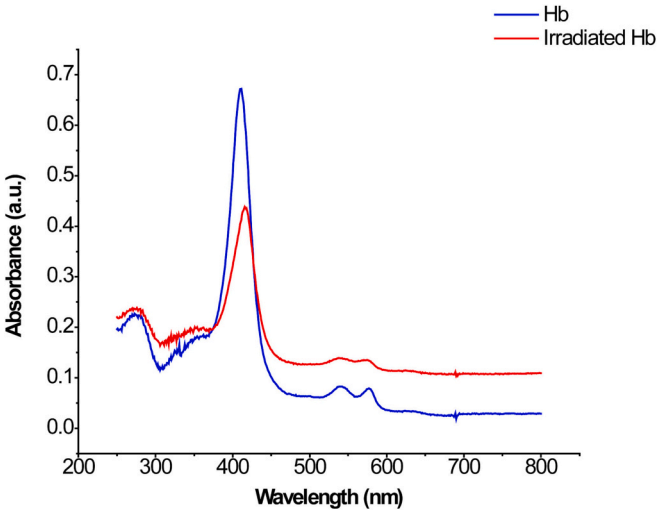

Fig. 4. Absorption spectra of Hb and the irradiated Hb thin layers. UV-VIS absorption spectra of intact Hb thin layer (blue) and irradiated Hb that contains the photoproduct (red line). All characteristics of absorption spectra are given in Table 1. (For interpretation of the references to colour in this figure legend, the reader is referred to the web version of this article.)

Table 1
Characteristics of Hb and Hb photoproduct UV-VIS absorption spectra. The mean and standard deviation of four separate absorbance measurements is represented.

Absorption band maximum position / intensity	Hb	Irradiated Hb region containing the photoproduct
λ_{max}^{UV} / nm	273 ± 2	272 ± 2
λ_{max}^{His} / nm	351 ± 2	351 ± 2
λ_{max}^{Soret} / nm	410 ± 2	417 ± 2
$\lambda_{max}^{Q\beta}$ / nm	539 ± 2	538 ± 2
$\lambda_{max}^{Q\alpha}$ / nm	577 ± 2	576 ± 2
A_{max}^{UV}	0.226 ± 0.003	0.237 ± 0.001
A_{max}^{His}	0.179 ± 0.008	0.200 ± 0.002
A_{max}^{Soret}	0.671 ± 0.002	0.438 ± 0.001
$A_{max}^{Q\beta}$	0.082 ± 0.007	0.139 ± 0.003
$A_{max}^{Q\alpha}$	0.079 ± 0.001	0.134 ± 0.003
A_{560}	0.063 ± 0.002	0.132 ± 0.005
$\Delta A_{Q\alpha}/\Delta A_{Q\beta} = (A_{max}^{Q\alpha} - A_{560})/(A_{max}^{Q\beta} - A_{560})$	0.804 ± 0.027	0.371 ± 0.014
$A_{max}^{Soret} / A_{max}^{Q\alpha}$	8.506 ± 0.046	3.254 ± 0.007
$A_{max}^{Soret} / A_{max}^{UV}$	2.962 ± 0.042	1.848 ± 0.014

[33–35]. In addition, excited by the different wavelengths one molecular species would give just the change in the fluorescence intensity while keeping the position of the spectral maximum fixed.

3.5. TPEF emission of PpIX

To characterize the Hb iron ion role in Hb photoproduct formation, TPEF spectra of PpIX were investigated. The obtained TPEF emission spectrum of PpIX (Fig. 6a black line) shows both distinctions and similarities to TPEF spectrum of the Hb photoproduct (Fig. 3e). Most notably, unlike Hb, PpIX is easily excited and TPEF emission is readily observed even at low irradiation intensities (Fig. 6a, black curve). However, the TPEF emission observed at low irradiation intensities originated predominantly from unaltered PpIX molecules, as evident from previously published data [36]. When using higher laser power (e.g., 16.5 mW), the TPEF emission spectrum of PpIX is considerably changed: becoming broader and with a maximum peak around 550 nm (Fig. 6a, blue curve), resembling the TPEF emission spectrum of the Hb photoproduct (Fig. 3e). This, in turn, suggests that intense irradiation of PpIX leads to the generation of PpIX photoproduct that is similar to the Hb photoproduct, so that iron atom is not necessary for the formation of Hb photoproduct.

3.6. TPEF emission of Hb treated with H_2O_2

It has been shown that Hb treatment with H_2O_2 also leads to the formation of a fluorescent product [27,28]. To determine whether similar photoproducts are formed under Hb treatment with H_2O_2 as upon its interaction with 730 nm ultrashort laser pulses, we compared how the TPEF intensity changed when increasing the exposure time (Fig. 6b) and TPEF spectra (Fig. 6c). Unlike for Hb thin film, where increase of fluorescence intensity and saturation were eventually observed (Fig. 6b, light green squares), the fluorescence of the H_2O_2-treated Hb shows a high TPEF emission intensity immediately upon excitation, even at the first exposure (Fig. 6b, olive dots). The increase of fluorescence in Hb film (Fig. 6b, light green) has the same trend as in erythrocytes (Fig. 2b). The slight discrepancy is due to different number of graph points and concentration of Hb in erythrocytes and thin Hb film. Moreover, the observed TPEF intensity was independent on the number of exposures, i.e., absorbed dose, of 730 nm ultrashort laser pulses. This confirms the hypothesis of the photodegradation of Hb involved in the photoproduct formation, since interaction between Hb and a 10 (or more) fold excess H_2O_2 leads to Hb degradation according to the [28]. Finally, the TPEF spectrum of H_2O_2-treated Hb thin film showed very good agreement with the TPEF spectra of Hb thin film treated with ultrashort laser pulses, the erythrocytes and the PpIX layer under high laser power, 16.5 mW (Fig. 6c).

Taken together, this suggests that upon Hb reaction with H_2O_2 and in the photochemical interaction of ultrashort laser pulses with Hb, the Hb photoproduct shows, at least with regard to TPEF emission, similar features. The overlap between the TPEF emission spectra of PpIX and Hb thin film suggests that heme, i.e., porphyrin rings photoexcitation playing a significant role in the Hb photoproduct formation. This could even include heme degradation, as already demonstrated within diseased so-called Köln erythrocytes', where observed fluorescence does not resemble that of porphyrins, chelated or otherwise, but does reveal some characteristics of dypirolic compound spectra [37]. Since dipyrrolic urinary pigments in patients with unstable hemoglobin disease are characterized and support the previous assumption regarding fluorescent Koln erythrocytes, it is more likely that under ultrashort laser pulses the heme's porphyrin ring breakage is enhanced. Importantly, fluorescent heme degradation products are already recognized as markers of red blood cell (RBC) oxidative stress [38], based on the original work of Nagababu and Rifkind, 1998, who have found that even small portion of the non-neutralized hydrogen peroxide in erythrocytes degrades the protoporphyrin and produce stable fluorescent heme degradation products. Nagababu and Rifkind 1998 reported two heme degradation products, one with an excitation wavelength of 321 nm and emission wavelength in the region of 465 nm and the second one with the excitation wavelength of 460 nm and emission wavelength in the region of 525 nm, based on the results that the same fluorescent bands were obtained after hydrogen peroxide treatment of heme or hemin. The broad emission spectra of a Hb photoproduct obtained in our study indicates that there are probably more than one Hb photoproduct species as well. The same authors [39] revealed that the mechanism for the generation of heme degradation products needs an initial reaction with hydrogen peroxide, producing Fe (IV) ferrylhemoglobin (ferrylHb) species, which further reacts with the second molecule of hydrogen peroxide producing superoxide radical, that can be retained longer in heme pocket than the superoxide formed during Hb autoxidation, and consequently initiating degradation of heme [28]. Namely, even in physiological conditions, RBCs are continuously exposed to both endogenous and exogenous sources of reactive oxygen species (ROS) (i.e., superoxide and hydrogen peroxide (H_2O_2)), which are mainly neutralized by the RBC antioxidant system. However, the autoxidation of Hb bound to the membrane is unavailable to the RBC antioxidant system which is mostly cytosolic. This process is especially pronounced when Hb is partially oxygenated, resulting in an increased rate of autoxidation and increased affinity for the RBC membrane, eventually affecting RBC deformability [38]. Even in fresh RBC samples heme degradation products can be found, and the amount of heme degradation increases in older RBCs [38]. Taking all these findings together, the interaction of ultrashort laser pulses with hemoglobin more likely accelerates the deoxygenation of hemoglobin and generation of superoxide radical, which affects heme, inducing the formation of stable fluorescent photoproduct.

3.7. Applications

3.7.1. Selective photo-labeling and live tracking of photo-labeled erythrocytes

Thanks to the high stability of the Hb photoproduct obtained upon interaction of the 730 nm ultrashort laser pulses with Hb molecules (Fig. 3d) and high spatiotemporal selectivity of our TPEF scanning microscope, we performed live tracking of individually labeled erythrocyte

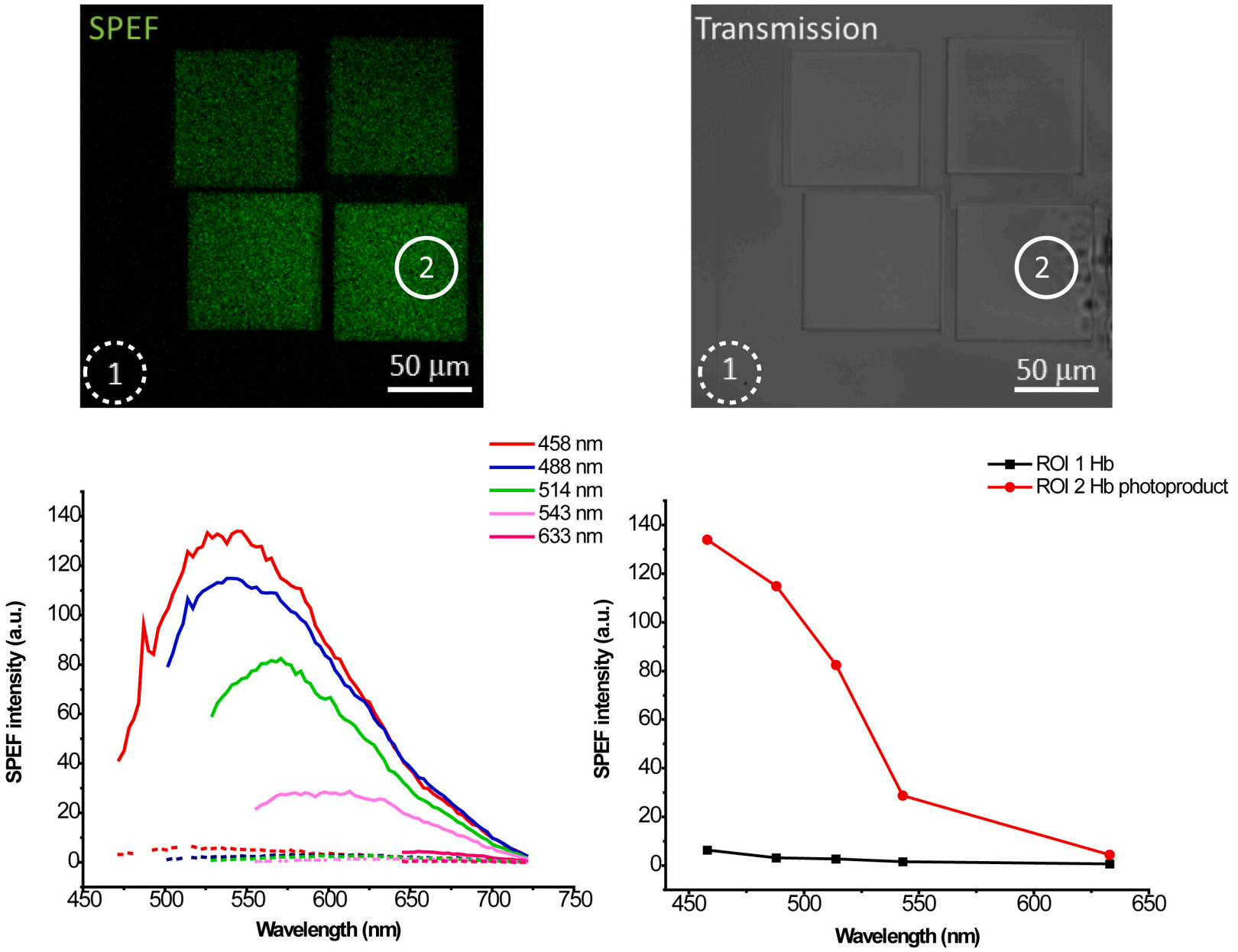

Fig. 5. Spectral imaging of Hb photoproduct patterns. (a) Single-photon excitation (SPEF) fluorescent image of the Hb photoproduct patterns recorded at 458 nm excitation, dashed circle represents region of interest (ROI 1) which is not irradiated by ultrashort pulsed laser beam under conditions needed for photoproduct formation, and solid circle represents ROI 2 which is irradiated by ultrashort pulsed laser beam, and it's clearly separate by photoproduct fluorescence emission, (b) Corresponding Bright-field image; (c) Single-photon excitation fluorescence spectra, read-out from ROI 1 (dashed line) for different excitation wavelengths and from ROI 2 (solid line); (d) Excitation efficiency: the emission intensity maxima at the different excitation wavelengths from ROI 1 Hb (untreated Hb) and ROI 2 (Hb photoproduct).

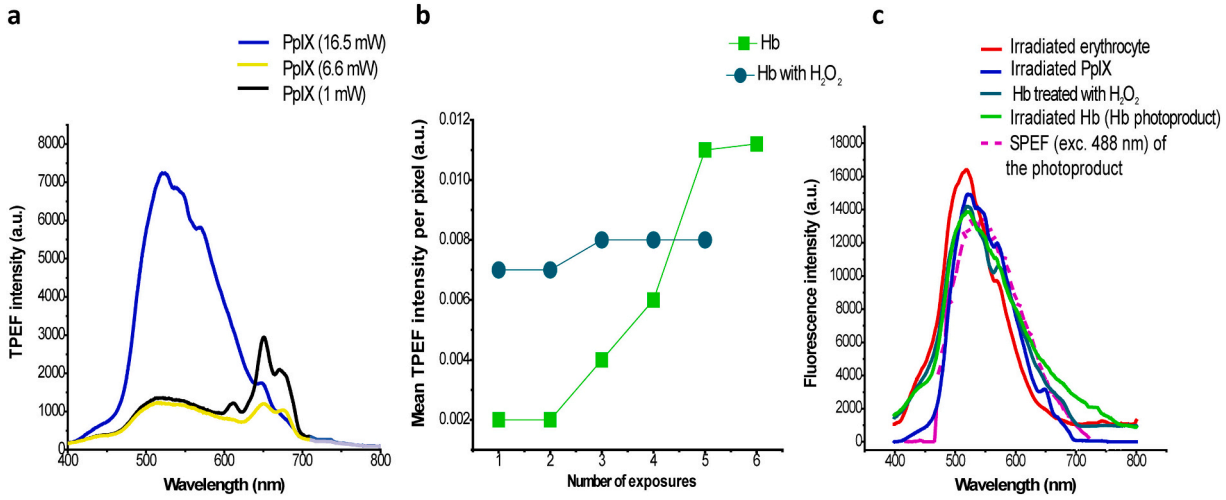

Fig. 6. TPEF spectra of PpIX and H_2O_2-treated Hb. (a) TPEF spectra of PpIX irradiated using different ultrashort pulsed laser powers (1.0 mW, black; 6.6 mW, yellow; 16.5 mW, dark blue); (b) Dependence of TPEF intensity vs. number of exposures in Hb thin film and H_2O_2-treated Hb thin film; (c) Overlapped TPEF spectra of Hb photoproduct (obtained in thin layer of Hb, green), the erythrocyte (red), thin layer PpIX under the laser power conditions (16.5 mW, blue), H_2O_2-treated Hb thin layer (cobalt blue) and Hb photoproduct SPEF spectrum (dashed purple). (For interpretation of the references to colour in this figure legend, the reader is referred to the web version of this article.)

(s) in vitro in the whole blood (Fig. 7 a-d). We present four timelapse images from the video (Supplemental Information) in which one erythrocyte is labeled by focused fs laser beam and then traced during its random motion. This was inspired by [11] where flow of the erythrocytes was shown in the vasculature of a whole, live animal but only with statical images, while we bring the dynamics of movement (Fig. 7 and corresponding video). Although the photo-labeling and tracking were performed in vitro, this method based on TPEF microscopy will enable to track with long-term period individual erythrocyte in a tissue [40] and blood vessel in laboratory animals, for instance in zebra fish [11] or even in mouse brain vasculature [41 – 43]. According to [41 – 43], where shadows of erythrocytes were traced in the blood flow in live animals through the cranial window using TPEF imaging, erythrocytes could be fluorescently activated by a fs laser beam and tracked through the vessels. In addition to selective photo-labeling of solely and deliberately chosen erythrocytes, that can be achieved by spatiotemporal control of the laser beam, but not by bulk H_2O_2 treatment, there are some more advantages of the presented method. Namely, treating the erythrocytes with H_2O_2 is rather uncontrollable in terms of targeted transformation of Hb only into the fluorescent molecule(s). H_2O_2 interact with other molecules in the erythrocytes' membrane and other structures which might be damaged or altered. Also, erythrocytes' morphology and related Hb distribution would be altered. Using the method of the laser photo-labeling presented in this work, only Hb molecules would be affected, and the erythrocytes would preserve their original morphology as well as its original Hb distribution which was already shown in [9]. The erythrocytes morphology and internal Hb distribution are one of key markers indicating the cell adaptation to physiological processes and their response to pathological conditions [9]. Eventually, the proposed method might have application for erythrocytes tracing in the blood vessels of the live animals even in imaging of highly bloodied and low transparent organs such as kidneys, since TPEF microscopy is extensively used nowadays for those purposes [41]. Prior investigations have unequivocally demonstrated that the morphology of erythrocytes can be studied using Two-Photon Excitation Fluorescence (TPEF) imaging, which enables examination of their oxygenation status [15], as well as distribution of Hb [9]. However, it is unclear whether the ultrashort laser pulses interferes with Hb's ability to perform its primary function of binding and releasing oxygen. In our present study, we establish that Hb undergoes alterations as a result of such interaction.

Having in mind the relationship of oxidative stress and hemoglobin, hemoglobin-based TPEF methodology is an emerging platform for the assessment of redox status of erythrocytes and their deformability under both physiological and pathophysiological conditions and even a broader spectrum of diseases that share the common feature of the appearance of extracellular hemoglobin or early cancer progression in means of neoangiogenesis. In this respect, photo acoustic microscopy can be employed for tracking of erythrocytes as suggested in [11] but with higher repetition rate lasers. Also, this technique can be used for investigation of oxygen saturation in the blood vessels [15].

3.7.2. *Pattern inscription (micropatterning) in Hb layer*

The long–term stability of the Hb photoproduct, its fluorescence and spatial precision of TPEF emission microscopy, enabled one more application – micro patterning of the Hb layer (Fig. 8). The inscribed patterns can stay fluorescent even for several months after being inscribed. In Fig. 8 a-d simple, spot-wise, patterns are presented in addition to the uniform square area. The spots were obtained from the diffraction limited focal volume and demonstrate the method limitation in terms of the spatial resolution. At each figure, a new spot-wise pattern was added, while the previous ones are still clearly visible. To demonstrate possibility and versatility of the method, as well as potential applications, we further wrote the letters “HEMMAGINERO” (dimensions 60 μm × 6 μm) in the Hb layer (Fig. 8e).

In terms of optical and spectroscopic response to the treatment with ultrashort laser pulses all mammalian [4,9,12,44,45] or even other vertebrates [46] Hb and erythrocytes are the same [47]. On the other hand, the slaughterhouses mammalian blood is a waste material from which Hb can be isolated in relatively low cost and relatively simple technological processes [48,49]. This might be a starting point for utilization of the Hb as the material for optical memories [50], hemoglobin-based therapeutics [51], intravital microscopy [52], conversion of micro fluorescent information into the document security or mass production of calibration samples in fluorescent microscopy [53–55]. Microscopic slides with fluorescent patterns are already commercially available [56] and broadly used for calibration and resolution measurements. While the fluorescence durability of the patterns in the existing materials remains unknown, we suggest Hb as a material for long lasting fluorescent patterns. In addition, the utilization of Hb from wasted slaughterhouse blood as the widely available material will be nature friendly since this material is considered to be severe pollutant [49].

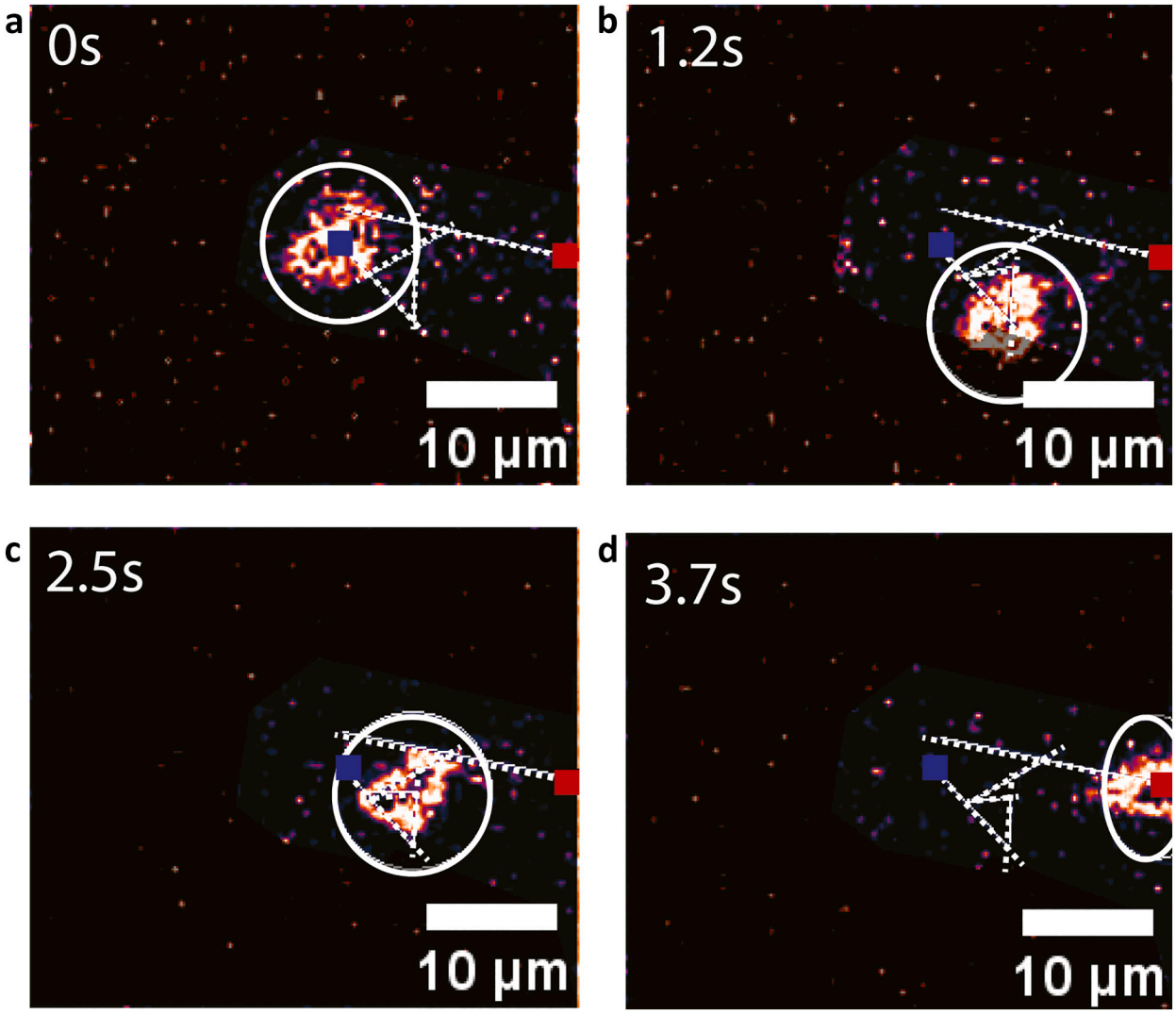

Fig. 7. Timelapse TPEF emission images of a single erythrocyte (encircled white). (a-d) Photo-labeled erythrocyte tracking in whole blood. The white dashed lines represent erythrocyte's trajectory with starting position (blue square) and final position (red square). (For interpretation of the references to colour in this figure legend, the reader is referred to the web version of this article.)

4. Conclusion

Using different spectroscopic techniques, in this study, we presented a novel insight into the photophysical properties of the fluorescent product emerged after exposure of Hb to 730 nm ultrashort laser pulses (hence Hb photoproduct) and its possible applications. We suggest that the interaction of the Hb with the ultrashort laser pulses in NIR region leads to the degradation of the Hb molecules and release of the iron, ending up with iron-free fluorescent species comparable to those emerged from the interaction of Hb with H_2O_2. Unlike the chemical interaction of Hb with H_2O_2 that occurs in bulk solution, using the tightly focused ultrashort pulsed laser beam the Hb photoproduct can be formed in spatiotemporal controllable manner without interaction with other molecules and erythrocytes structures (e.g. membrane). In other words, we can irradiate selected erythrocytes solely, and the laser pulses will alter primarily Hb, but not the other molecules. We inscribed sub-micrometer fluorescent patterns on a Hb thin film by the spatiotemporal control, of ultrashort pulsed laser beam. We have also induced the Hb photoproduct formation in a single human healthy erythrocyte making them fluorescent in the sample of whole blood and track their movement in space and time. The present study could contribute towards understanding photophysical properties of photoproduct, formed by the interaction of ultrashort laser pulses with Hb and erythrocytes, establishing a foundation for the future progress in the field of bio-derived biomaterials.

Supplementary data to this article can be found online at https://doi.org/10.1016/j.ijbiomac.2023.125312.

CRediT authorship contribution statement

M. Radmilović prepared the samples, performed TPEF imaging, TPEF spectra measurements and absorption spectra measurements, erythrocytes tracking, Hb micro-patterning, and prepared all the images; I. Drvenica prepared the samples and supervised Hb and erythrocytes isolation, managed the research; M. Rabasović constructed the TPEF experimental setup, supervised the TPEF imaging and spectra measurements, managed the research; V. Ilić supervised sample preparation, managed the research; D. Pavlović prepared the samples and imaged the erythrocytes by TPEF microscopy and measured absorption spectra; S. Oasa performed spectral imaging; V. Vukojević supervised spectral imaging; M. Perić performed confocal imaging; S. Nikolić maintained TPEF experimental setup and modified the imaging software; A. Krmpot constructed the TPEF experimental setup, supervised the measurements, managed the research. All the authors wrote and reviewed the

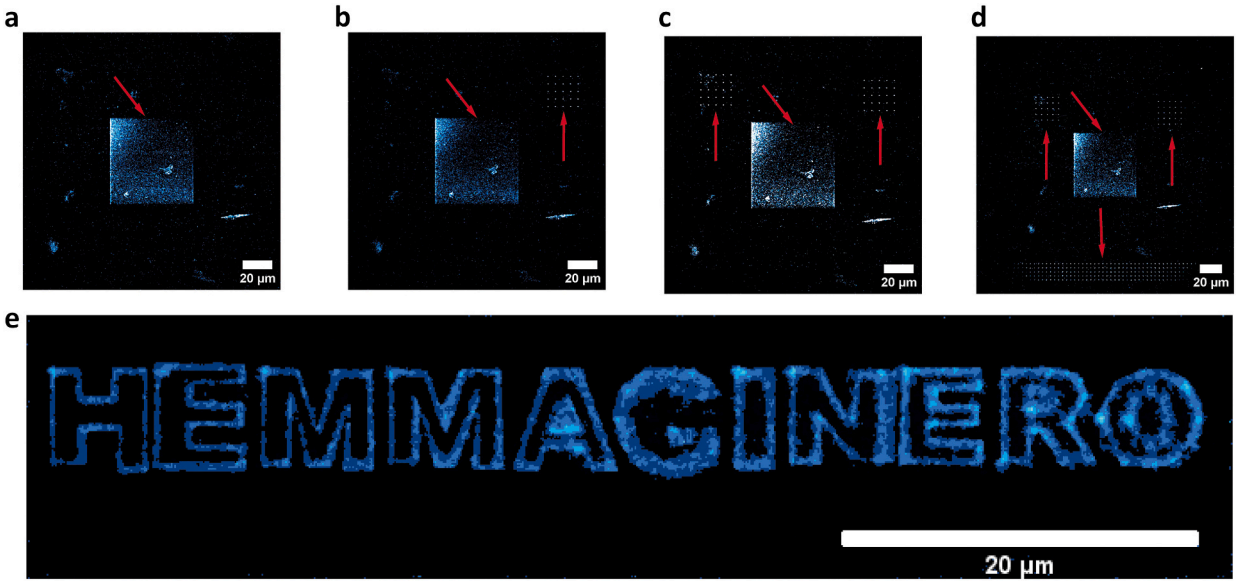

Fig. 8. Micropattering in Hb layer by fs laser pulses. (a-d) Arbitrary uniform and spot-wise patterns (red arrow pointed) inscribed in the thin Hb film by ultrashort laser pulses. The patterns exhibit increased TPEF signal (marked by red arrows). (e) Fluorescent Hb photoproduct in the form of letters pattern. (For interpretation of the references to colour in this figure legend, the reader is referred to the web version of this article.)

manuscript. This article is a part of M. Radmilović's PhD thesis.

Declaration of competing interest

The authors declare that they have no known competing financial interests or personal relationships that could have appeared to influence the work reported in this paper.

Data availability

Data will be made available on request.

Acknowledgement

We would like to thank to Milan Minić, Institue of Physics Belgrade for the technical support and to the staff of the Center for Laser Microcopy, Faculty of Biology, University of Belgrade, Serbia. This work was supported by the Science Fund of the Republic of Serbia [program PROMIS, project HEMMAGINERO, grant number 6066079] and Qatar National Research Fund [grant number PPM 04-0131-200019]. The authors acknowledge funding provided by the Institute of Physics Belgrade, through the grant by the Ministry of Education, Science and Technological Development of the Republic of Serbia and the Institute for Medical Research University of Belgrade, National Institute of the Republic of Serbia, through the contract No. 451-03-47/2023-01/200015.

References

[1] L. Kiger, C. Vasseur, E. Domingues-Hamdi, G. Truan, M.C. Marden, V. Baudin-Creuza, Dynamics of α-Hb chain binding to its chaperone AHSP depends on heme coordination and redox state, Biochim. Biophys. Acta - Gen. Subj. 2014 (1840) 277–287, https://doi.org/10.1016/j.bbagen.2013.09.015.
[2] M. Weissbluth, Hemoglobin, Springer, Berlin, 1974, pp. 10–26.
[3] Q. Sun, W. Zheng, J. Wang, Y. Luo, J.Y. Qu, Mechanism of two-photon excited hemoglobin fluorescence emission, J. Biomed. Opt. 20 (2015) 105014, https://doi.org/10.1117/1.JBO.20.10.105014.
[4] W. Zheng, D. Li, Y. Zeng, Y. Luo, J.Y. Qu, W.R. Zipfel, R.M. Williams, R. Christie, A. Y. Nikitin, B.T. Hyman, W.W. Webb, Two-photon excited hemoglobin fluorescence, Biomed. Opt. Express 2 (2011) 71–79, https://doi.org/10.1364/BOE.2.000071.
[5] G.O. Clay, A.C. Millard, C.B. Schaffer, J. Aus-der-Au, P.S. Tsai, J.A. Squier, D. Kleinfeld, Spectroscopy of third-harmonic generation: evidence for resonances in model compounds and ligated hemoglobin, J. Opt. Soc. Am. B. 23 (2006) 932, https://doi.org/10.1364/josab.23.000932.
[6] G.O. Clay, C.B. Schaffer, D. Kleinfeld, Large two-photon absorptivity of hemoglobin in the infrared range of 780-880 nm, J. Chem. Phys. 126 (2007) 01B609, https://doi.org/10.1063/1.2404678.
[7] N.L. Garrett, A. Lalatsa, I. Uchegbu, A. Schätzlein, J. Moger, Exploring uptake mechanisms of oral nanomedicines using multimodal nonlinear optical microscopy, J. Biophotonics 5 (2012) 458–468, https://doi.org/10.1002/jbio.201200006.
[8] G.D. Vigil, S.S. Howard, Photophysical characterization of sickle cell disease hemoglobin by multi-photon microscopy, Biomed. Opt. Express 6 (2015) 4098–4104, https://doi.org/10.1364/boe.6.004098.
[9] K. Bukara, S.Z. Jovanić, I.T. Drvenica, A. Stančić, V. Ilić, M.D. Rabasović, D. V. Pantelić, B.M. Jelenković, B. Bugarski, A.J. Krmpot, Mapping of hemoglobin in erythrocytes and erythrocyte ghosts using two photon excitation fluorescence microscopy, J. Biomed. Opt. 22 (2017) 026003, https://doi.org/10.1117/1.jbo.22.2.026003.
[10] D. Li, W. Zheng, Y. Zeng, Y. Luo, J.Y. Qu, Two-photon excited hemoglobin fluorescence provides contrast mechanism for label-free imaging of microvasculature in vivo, Opt. Lett. 36 (2011) 834–836, https://doi.org/10.1364/OL.36.000834.
[11] Y. Zeng, J. Xu, D. Li, L. Li, Z. Wen, J.Y. Qu, Label-free in vivo flow cytometry in zebrafish using two-photon autofluorescence imaging, Opt. Lett. 37 (2012) 2490–2492, https://doi.org/10.1364/OL.37.002490.
[12] D. Li, W. Zheng, S.K. Teh, Y. Zeng, Y. Luo, J.Y. Qu, Time-resolved detection enables standard two-photon fluorescence microscopy for in vivo label-free imaging of microvasculature in tissue, Opt. Lett. 36 (2011) 2638–2640, https://doi.org/10.1364/OL.36.002638.
[13] R. Podlipec, J. Mur, J. Petelin, J. Štrancar, R. Petkovšek, Two-photon retinal theranostics by adaptive compact laser source, Appl. Phys. A Mater. Sci. Process. 126 (2020) 1–9, https://doi.org/10.1007/s00339-020-03587-2.
[14] R.L. Shelton, S.P. Mattison, B.E. Applegate, Volumetric imaging of erythrocytes using label-free multiphoton photoacoustic microscopy, J. Biophotonics 7 (2014) 834–840, https://doi.org/10.1002/jbio.201300059.
[15] Y. Wang, S. Hu, K. Maslov, Y. Zhang, Y. Xia, L.V. Wang, In vivo integrated photoacoustic and confocal microscopy of hemoglobin oxygen saturation and oxygen partial pressure, Opt. Lett. 36 (2011) 1029, https://doi.org/10.1364/ol.36.001029.
[16] J.J. Yao, L.V. Wang, Photoacoustic microscopy, Laser Photonics Rev. 7 (2013) 758–778.
[17] G.J. Tserevelakis, M. Pavlidis, A. Samaras, G.D. Barmparis, K.G. Mavrakis, I. Draganidis, A. Oikonomou, E. Fanouraki, G.P. Tsironis, G. Zacharakis, Hybrid confocal fluorescence and photoacoustic microscopy for the label-free investigation of melanin accumulation in fish scales, Sci. Rep. 12 (2022) 1–14, https://doi.org/10.1038/s41598-022-11262-0.
[18] I. Saytashev, R. Glenn, G.A. Murashova, S. Osseiran, D. Spence, C.L. Evans, M. Dantus, Multiphoton excited hemoglobin fluorescence and third harmonic generation for non-invasive microscopy of stored blood, Biomed. Opt. Express 7 (2016) 3449–3460, https://doi.org/10.1364/boe.7.003449.
[19] M.E. Reinhard, M.W. Mara, T. Kroll, H. Lim, R.G. Hadt, R. Alonso-Mori, M. Chollet, J.M. Glownia, S. Nelson, D. Sokaras, K. Kunnus, T.B. van Driel, R.W. Hartsock, K. S. Kjaer, C. Weninger, E. Biasin, L.B. Gee, K.O. Hodgson, B. Hedman, U. Bergmann,

E.I. Solomon, K.J. Gaffney, Short-lived metal-centered excited state initiates iron-methionine photodissociation in ferrous cytochrome c, Nat. Commun. 12 (2021) 1–8, https://doi.org/10.1038/s41467-021-21423-w.
[20] https://www.ncbi.nlm.nih.gov/pmc/articles/PMC3822757/.
[21] J.G. Mohanty, E. Nagababu, J.M. Rifkind, Red blood cell oxidative stress impairs oxygen delivery and induces red blood cell aging, Front. Physiol. 5 (2014) 1–6, https://doi.org/10.3389/fphys.2014.00084.
[22] S. Sun, A. Lv, S. Li, C. Zhao, Q. Chen, Z. Li, Y. Wang, A. Wu, H. Lin, Biomolecule-based stimuli-responsive nanohybrids for tumor-specific and cascade-enhanced synergistic therapy, Acta Biomater. 152 (2022) 484–494, https://doi.org/10.1016/j.actbio.2022.08.038.
[23] A.I. Alayash, Oxygen therapeutics: can we tame haemoglobin? Nat. Rev. Drug Discov. 3 (2004) 152–159, https://doi.org/10.1038/nrd1307.
[24] D. Chakraborty, S. Sarkar, P.K. Das, Blood dots: hemoglobin-derived carbon dots as hydrogen peroxide sensors and pro-drug activators, ACS Sustain. Chem. Eng. 6 (2018) 4661–4670, https://doi.org/10.1021/acssuschemeng.7b03691.
[25] S. Li, W. Sun, M. Ouyang, B. Yu, Y. Chen, Y. Wang, D. Zhou, Hemoglobin-related biomaterials and their applications, Adv. NanoBiomed Res. 2200103 (2022) 1–12, https://doi.org/10.1002/anbr.202200103.
[26] E.A. Shirshin, B.P. Yakimov, S.A. Rodionov, N.P. Omelyanenko, A.V. Priezzhev, V. V. Fadeev, M.E. Darvin, Formation of hemoglobin photoproduct is responsible for two-photon and single photon-excited fluorescence of red blood cells, Laser Phys. Lett. 15 (2018), 075604, https://doi.org/10.1088/1612-202X/aac003.
[27] E. Nagababu, J.M. Rifkind, Formation of fluorescent heme degradation products during the oxidation of hemoglobin by hydrogen peroxide, Biochem. Biophys. Res. Commun. 247 (1998) 592–596, https://doi.org/10.1006/bbrc.1998.8846.
[28] E. Nagababu, J.M. Rifkind, Reaction of hydrogen peroxide with ferrylhemoglobin: superoxide production and heme degradation, Biochemistry. 39 (2000) 12503–12511, https://doi.org/10.1021/bi992170y.
[29] A.Z. Stančić, I.T. Drvenica, H.N. Obradović, B.M. Bugarski, V.L. Ilić, D.S. Bugarski, Native bovine hemoglobin reduces differentiation capacity of mesenchymal stromal cells in vitro, Int. J. Biol. Macromol. 144 (2020) 909–920, https://doi.org/10.1016/j.ijbiomac.2019.09.167.
[30] M.D. Rabasović, D.V. Pantelić, B.M. Jelenković, S.B. Ćurčić, M.S. Rabasović, M. D. Vrbica, V.M. Lazović, B.P.M. Ćurčić, A.J. Krmpot, Nonlinear microscopy of chitin and chitinous structures: a case study of two cave-dwelling insects, J. Biomed. Opt. 20 (2015) 016010, https://doi.org/10.1117/1.jbo.20.1.016010.
[31] T. Lainović, J. Margueritat, Q. Martinet, X. Dagany, L. Blažić, D. Pantelić, M. D. Rabasović, A.J. Krmpot, T. Dehoux, Micromechanical imaging of dentin with Brillouin microscopy, Acta Biomater. 105 (2020) 214–222, https://doi.org/10.1016/j.actbio.2020.01.035.
[32] N.S. Selim, S.M. El-marakby, Radiation-induced changes in the optical properties of hemoglobin molecule, Spectrochim. Acta A Mol. Biomol. Spectrosc. 76 (2010) 56–61, https://doi.org/10.1016/j.saa.2010.02.046.
[33] E.K. Hanson, J. Ballantyne, A blue spectral shift of the hemoglobin soret band correlates with the age (time since deposition) of dried bloodstains, PLoS One 5 (2010) 1–11, https://doi.org/10.1371/journal.pone.0012830.
[34] I.T. Drvenica, A.Z. Stančić, A.M. Kalušević, S.B. Marković, J.J. Dragišić Maksimović, V.A. Nedović, B.M. Bugarski, V.L. Ilić, Maltose-mediated, long-term stabilization of freeze- and spray-dried forms of bovine and porcine hemoglobin, J. Serb. Chem. Soc. 84 (2019) 1105–1117, https://doi.org/10.2298/JSC190513067D.
[35] C. Bonaventura, R. Henkens, A.I. Alayash, S. Banerjee, A.L. Crumbliss, Molecular controls of the oxygenation and redox reactions of hemoglobin, Antioxid. Redox Signal. 18 (2013) 2298–2313, https://doi.org/10.1089/ars.2012.4947.
[36] H. Lu, F. Floris, M. Rensing, S. Andersson-Engels, Fluorescence spectroscopy study of protoporphyrin IX in optical tissue simulating liquid phantoms, Materials (Basel) 13 (2020) 7–16, https://doi.org/10.3390/ma13092105.
[37] S.M. Waugh, P.S. Low, Hemichrome binding to band 3: nucleation of Heinz bodies on the erythrocyte membrane, Biochemistry. 24 (1) (1985) 34–39, https://doi.org/10.1021/bi00322a006.
[38] J.G. Mohanty, E. Nagababu, J.M. Rifkind, Red blood cell oxidative stress impairs oxygen delivery and induces red blood cell aging, Front. Physiol. 5 (2014) 1–6, https://doi.org/10.3389/fphys.2014.00084.
[39] E. Nagababu, S. Ramasamy, J.M. Rifkind, Y. Jia, A.I. Alayash, Site-specific cross-linking of human and bovine hemoglobins differentially alters oxygen binding and redox side reactions producing rhombic heme and heme degradation, Biochemistry. 41 (2002) 7407–7415, https://doi.org/10.1021/bi0121048.
[40] U.N. Shroff, I.M. Schiessl, G. Gyarmati, A. Riquier-Brison, J. Peti-Peterdi, Novel fluorescence techniques to quantitate renal cell biology, Methods Cell Biol. 154 (2019) 85–107, https://doi.org/10.1016/bs.mcb.2019.04.013.
[41] D. Sardella, A.M. Kristensen, L. Bordoni, H. Kidmose, A. Shahrokhtash, D. S. Sutherland, S. Frische, I.M. Schiessl, Serial Intravital 2-photon Microscopy and Analysis of the Kidney Using Upright Microscopes, 2023, pp. 1–17, https://doi.org/10.3389/fphys.2023.1176409.
[42] E. Gutiérrez-jiménez, H. Angleys, P.M. Rasmussen, M.J. West, L. Catalini, N. K. Iversen, M.S. Jensen, S. Frische, L. Østergaard, Disturbances in the control of capillary flow in an aged APPswe/PS1ΔE9 model of Alzheimer's disease, Neurobiol. Aging 62 (2018) 82–94, https://doi.org/10.1016/j.neurobiolaging.2017.10.006.
[43] E. Gutiérrez-jiménez, C. Cai, I.K. Mikkelsen, P.M. Rasmussen, H. Angleys, M. Merrild, K. Mouridsen, S.N. Jespersen, J. Lee, N.K. Iversen, S. Sakadzic, L. Østergaard, Effect of electrical forepaw stimulation on capillary transit-time heterogeneity (CTH), J. Cereb. Blood Flow Metab. 36 (2016) 2072–2086, https://doi.org/10.1177/0271678X16631560.
[44] T. Wu, J. Liao, J. Yu, Y. Gao, H. Li, J. Wu, X. Xia, K. Shi, W. Zheng, In vivo label-free two-photon excitation autofluorescence microscopy of microvasculature using a 520 nm femtosecond fiber laser, Opt. Lett. 45 (2020) 2704–2707, https://doi.org/10.1364/OL.394242.
[45] S. He, C. Ye, Q. Sun, C.K.S. Leung, J.Y. Qu, Label-free nonlinear optical imaging of mouse retina, Biomed. Opt. Expr. 6 (2015) 2459–2465, https://doi.org/10.1364/BOE.6.001055.
[46] Y. Zeng, J. Xu, D. Li, L. Li, Z. Wen, J.Y. Qu, Label-free in vivo flow cytometry in zebrafish using two-photon autofluorescence imaging, Opt. Lett. 37 (2012) 2490–2492, https://doi.org/10.1364/OL.37.002490.
[47] J.F. Ortas, P. Mahou, S. Escot, C. Stringari, N.B. David, L. Bally-Cuif, N. Dray, M. Négrerie, W. Supatto, E. Beaurepaire, Label-free imaging of red blood cells and oxygenation with color third-order sum-frequency generation microscopy, Light Sci. Appl. 12 (2023), https://doi.org/10.1038/s41377-022-01064-4.
[48] I.T. Kostić, V.L. Ilić, V.B. Dordević, K.M. Bukara, S.B. Mojsilović, V.A. Nedović, D. S. Bugarski, D.N. Veljović, D.M. Mišić, B.M. Bugarski, Erythrocyte membranes from slaughterhouse blood as potential drug vehicles: isolation by gradual hypotonic hemolysis and biochemical and morphological characterization, Colloids Surf. B Biointerfaces. 122 (2014) 250–259, https://doi.org/10.1016/j.colsurfb.2014.06.043.
[49] C.S.F. Bah, A.E.D.A. Bekhit, A. Carne, M.A. Mcconnell, Slaughterhouse blood: an emerging source of bioactive compounds, Compr. Rev. Food Sci. Food Saf. 12 (2013) 314–331, https://doi.org/10.1111/1541-4337.12013.
[50] L.A. Frolova, Y. Furmansky, A.F. Shestakov, N.A. Emelianov, P.A. Liddell, D. Gust, I. Visoly-Fisher, P.A. Troshin, Advanced nonvolatile organic optical memory using self-assembled monolayers of porphyrin-fullerene dyads, ACS Appl. Mater. Interfaces 14 (2022) 15461–15467, https://doi.org/10.1021/acsami.1c24979.
[51] P. Charoenphol, K. Oswalt, C.J. Bishop, Therapeutics incorporating blood constituents, Acta Biomater. 73 (2018) 64–80, https://doi.org/10.1016/j.actbio.2018.03.046.
[52] W. Choe, A.P. Acharya, B.G. Keselowsky, B.S. Sorg, Intravital microscopy imaging of macrophage localization to immunogenic particles and co-localized tissue oxygen saturation, Acta Biomater. 6 (2010) 3491–3498, https://doi.org/10.1016/j.actbio.2010.03.006.
[53] I. Begemann, A. Viplav, C. Rasch, M. Galic, Stochastic micro-pattern for automated correlative fluorescence - scanning electron microscopy, Nat. Publ. Gr. (2015) 1–12, https://doi.org/10.1038/srep17973.
[54] L. Benedetti, E. Sogne, S. Rodighiero, D. Marchesi, P. Milani, M. Francolini, Customized patterned substrates for highly versatile correlative light-scanning electron microscopy, Sci. Rep. 4 (2014) 7033, https://doi.org/10.1038/srep07033.
[55] A.D. Corbett, M. Shaw, A. Yacoot, A. Jefferson, L. Schermelleh, T. Wilson, M. Booth, P.S. Salter, Microscope Calibration Using Laser Written Fluorescence 26, 2018, pp. 21887–21900, https://doi.org/10.1364/OE.26.021887.
[56] https://www.psfcheck.com/psfcheck-slides.